Matrix Microcracking Effect on the Structural Response of a Thermal Protection System

Sarah L. Langston[1]

NASA Langley Research Center, Hampton, VA, 23681, USA

Keith H. Peterson[2]

NASA Ames Research Center, Moffett Field, CA, 94035, USA

Carl C. Poteet[3]

NASA Langley Research Center, Hampton, VA, 23681, USA

The effect of microcracking in the phenolic matrix of a three-dimensional woven thermal protection system (TPS) and resulting material stiffness reduction was studied via a comparison of finite element results from linear and iterative linear analyses. A dual-layer continuous dry weave material with a low-density phenolic resin matrix has been developed for use in extreme environments. Due to high stresses in the through-the-thickness direction, microcracks may form in the matrix. The matrix does not have structural load transfer requirements, and testing has shown that microcracked phenolic resin satisfies thermal requirements. Microcracks in the matrix would result in a reduction of stiffness, which could alter the structural performance. A study was conducted to determine if reduction in material stiffness would change the load paths or structural margins. A linear finite element analysis that did not account for microcracking and an iterative linear finite element analysis that accounted for propagation microcracks [4]were compared. Four subcases were analyzed with

Presented at the AIAA SciTech 2019 Forum, Januaray 7-11, 2019, San Diego, California, AIAA 2019-0162
[1] Research Aerospace Engineer, Structural Mechanics and Concepts Branch, MS 190, AIAA member.
[2] Aerospace Engineer, Thermal Protection Materials Branch, MS 234:118
[3] Research Aerospace Engineer, Structural Mechanics and Concepts Branch, MS 190

results indicating that the assumed propagation strength for the microcracking is the critical parameter for determining the extent of microcracking. Phenolic microcracking does not appear to have an adverse effect on the structural response and is not a critical failure for the modeled TPS.

I. Introduction

Delivering payloads to the surface of other planets requires spacecraft to travel through the planet's atmosphere. The extreme aerodynamic heating experienced by an object entering these atmospheres requires the use of thermal protection systems (TPS) on spacecraft to protect the payload from the resulting high temperatures. Depending on the entry environment (atmosphere density, atmosphere composition, speed of the vehicle, etc.), different types of TPS are necessary [1]. Entry into planet atmospheres with extreme environments, such as Venus or Saturn, requires an ablative TPS. Ablators are a type of semi-passive TPS that are able to withstand high heating rates, and because they absorb heat through ablation, they are a single-use TPS [1]. Several types of ablative TPS have been flown on NASA missions. Those ablators include: superlight ablators (SLA) [2], Phenolic Impregnated Carbon Ablator (PICA) [3], and AVCOAT [4]. SLA and PICA were used successfully as the TPS for the Mars Science Laboratory (MSL) mission [5,6]. AVCOAT was used during the Apollo program, where the material was infused into a honeycomb substructure [4,7]. AVCOAT was also used on the Orion spacecraft, and was sucesfully implemented on the first flight test of the vehicle, named Exploration Flight Test 1 (EFT-1). The Orion spacecraft uses an updated AVCOAT forumulation and all subsequent Orion spacecraft will install the material in blocks, rather than the injection into a honeycomb structure used on the Apollo vehicles and EFT-1.

The Heatshield for Extreme Entry Environment Technology (HEEET) project is a multi-year endeavor to increase the technology readiness level (TRL) of a novel three-dimensional (3-D) woven TPS. The 3-D woven TPS is designed for extreme entry conditions and is mission-enabling: able to withstand high heat fluxes and entry pressures such as those on Venus, Saturn, Ice Giants, or high-speed sample return to Earth missions; and able to be tailored in thickness for each mission. Currently, missions to these planets are mass-limited due to the need to use fully-dense carbon phenolic for the TPS. The 3-D woven TPS is able to withstand similar pressures and heating rates as fully dense carbon phenolic but at a lower mass, opening the trade space for missions to these planets or other missions with similar heating rate requirements. A project goal was to raise the TRL from approximately three to six, which required a

subsystem test of the technology in a relevant environment. Relevant environments for TPS would include launch loads, on-orbit transit in space, and atmospheric entry. To meet the goal of TRL 6, the HEEET project designed and built a 39-inch diameter heatshield for ground testing.

Progressive damage analysis has been used in analysis of composites at many different length scales from micromechanical up to structural [9,10]. At the mesoscale level, Continuum Damage Mechanics (CDM) [11] is often used, where damange can be represented as a reduction of stiffness [12]. While CDM is a very useful tool, experimental work has shown that many factors must be taken into account when using the technique in finite element analysis [13]. Due to the complexity, CDM has been expanded upon in recent years, as well as additional methods used to accurately model and predict damage in composite materials [9].

While the majority of the reseach for progressive damange analysis has been performed on fracture-critical structural composites and typically not required on the non-structural TPS components of most vehicles, the techniques can still be useful in TPS structural analysis. For instance, the basic principles of CDM, where damage or microcracks in a material can be represented as a reduction of stiffness in a material, can be used as an analysis technique in some TPS materials. The HEEET TPS material (to be described in the following section) is a good candidate for this as the material is a composite. The study presented in this paper was to be a preliminary study into the potential effects of microcracking of the matrix material of the HEEET TPS, where the microcracked material would be represented as a reduced stiffness material. The primary purpose of this exploratory study was to determine if potential microcracks within the material matrix might effect the structural response of the entire test article, even away from the microcracked material. Of particular importance would be any findings that indicated a change in the load paths or the reductions of any structural margins on the test article which had the possibility to influence testing decisions.

II. HEEET Material

The 3-D woven TPS, henceforth referred to as HEEET, is a 3-D layer-to-layer woven composite material. HEEET has a dual-layer architecture consisting of an outer recession layer and an inner insulating layer. The recession layer is comprised of densely woven carbon fibers. The function of the recession layer is to ablate and manage ablation during planetary entry. The insulating layer is a lower-density weave of blended carbon and phenolic yarn. The function of the insulation layer is to maintain the internal temperature below the maximum allowable. Due to the layer-

to-layer weave, there are continuously woven fibers in the through-the-thickness (TTT) direction of the material. The addition of these TTT fibers leads to an increased toughness in the TTT direction compared to ablative TPS material without continuous TTT fibers [14]. HEEET is woven in a single piece as a conformable dry weave. The dry weave is then infiltrated with low-density phenolic resin, which forms the porous phenolic matrix of HEEET. The blended yarn, the dry weave on the loom, the conformable dry weave, and the phenolic resin-infused final HEEET are shown in Figure 1.

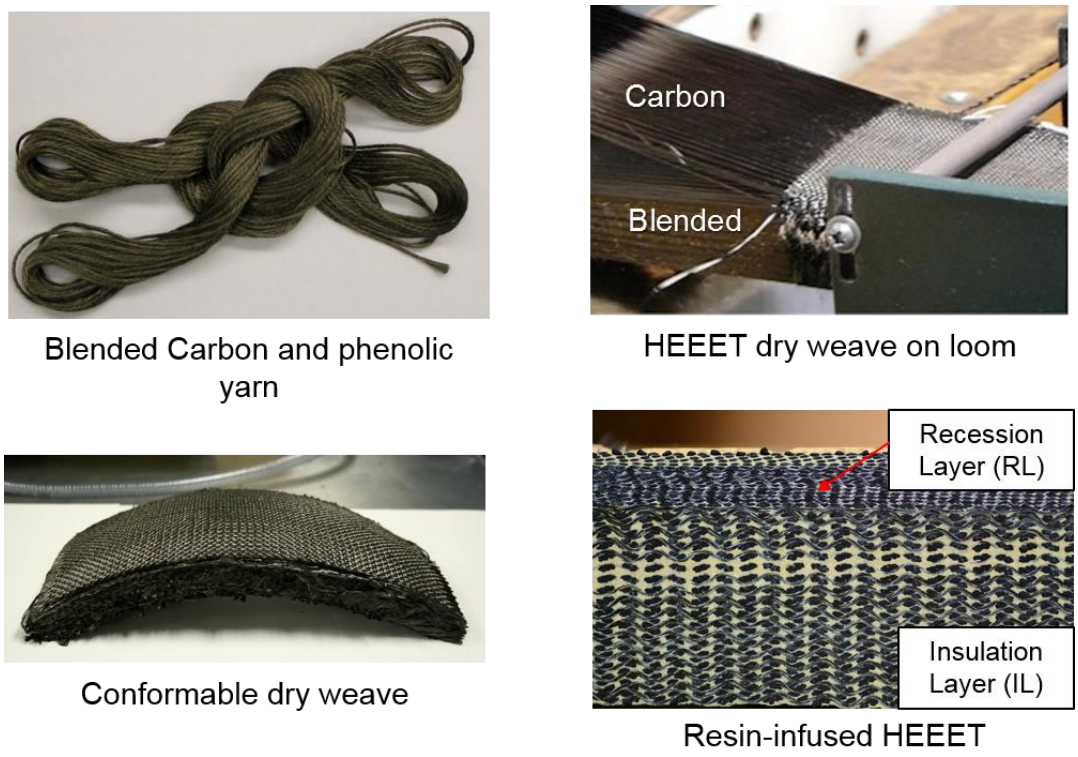

Figure 1. Clockwise from the upper left: The blended yarn constituent of the insulation layer, the HEEET dry weave on the loom, the resin-infused final HEEET material, and the conformable dry weave.

The function of the phenolic matrix is to block the flow of hot gases into the material and insulate the internal surface from excessive temperatures. There are no load transfer requirements for the matrix, as the fibers are intended to carry the mechanical load. Testing has shown that microcracked matrix material can fully satisfy the thermal requirements to block flow and provide adequate insulation. Testing has also shown that microcracks within the phenolic are likely to form in the TTT direction under certain loading conditions [14]. Examples of phenolic microcracking seen on a magnified image are shown in Figure 2.

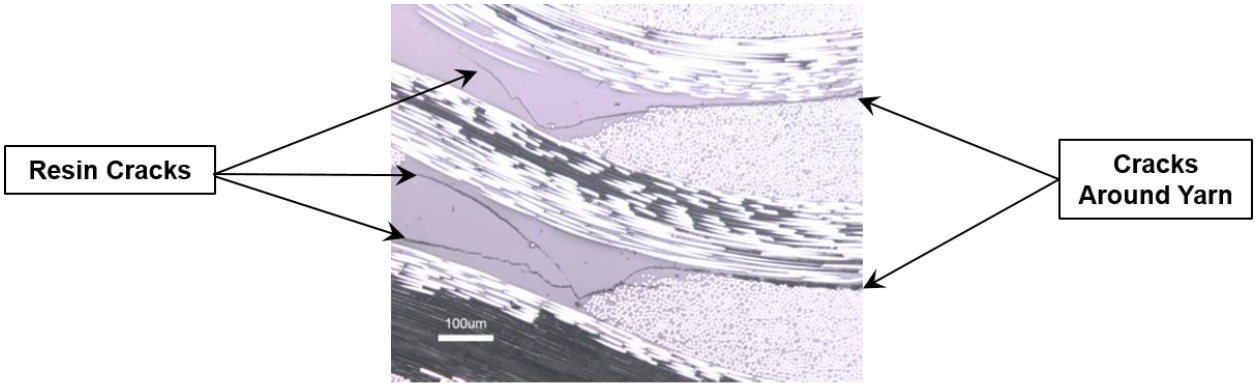

Figure 2. Polished microscopic image of the HEEET material with phenolic microcracks.

Manufacturing limitations on the width of the dry weave that can be produced drive the need for tiled heatshield architectures. In a tiled heatshield architecture, compliance is needed in the material system to reduce the bondline stresses between the tiles, thus a gap filler between the tiles is necessary. Phenolic resin cracking is used as a feature in the compliant gap filler created from HEEET to increase the compliance in the material system. Microcracked matrix in all derivatives of the HEEET material increases the compliance of the material while the fibers remain intact and provide cohesion of the material. Because microcracking does not prevent the matrix from satisfying the thermal requirement and microcracking of the matrix does not lead to critical structural failure of the material system, microcracking is not considered a material failure.

III. Engineering Test Unit

The engineering test unit (ETU) is a representative 39-inch diameter heatshield designed for a nominal Saturn mission. The test article is a 45° sphere-cone with an outer mold line shoulder radius of four inches. The heatshield is comprised of a composite carrier structure that HEEET is bonded to and an internal metallic ring for additional structural support and ground support equipment attachment. The HEEET material bonded to the exterior of the composite carrier structure consists of acreage HEEET tiles, as well as compliant gap filler and close-out plugs. The compliant gap filler and close-out plugs are created using the parent HEEET material. Further reference to HEEET in the current paper will continue to refer to the HEEET material used in the acreage tiles described in Section II. The ETU and the ETU components are shown in Figure 3.

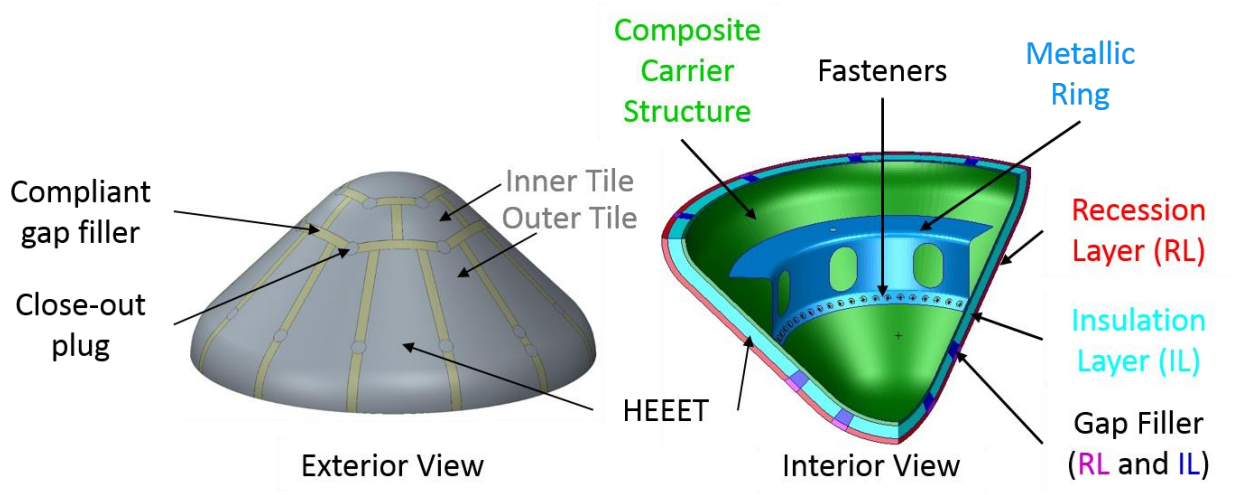

Figure 3. ETU exterior and cross-section with system components labeled.

IV. Finite Element Analysis of the ETU

While phenolic microcracking in the matrix is not considered a failure, understanding the effect of the reduction of stiffness in the material on the structural response of the system is important. Prior analysis had indicated that high stress zones within the material would produce phenolic microcracks primarily in the TTT direction and that microcracking leads to a localized material stiffness reduction and could change the stress state in this localized region [14]. However, the effect of the microcracks on the structural response of the entire ETU away from the reduced stiffness regions was unknown.

In order to preliminarily investigate the effect of the localized material stiffness reduction on the entire structural response of the ETU, an exploratory study was performed. The study compared a linear finite element analysis that assumed pristine material stiffness with an iterative linear finite element analysis which included propagating material stiffness reduction in the insulating layer of the HEEET. The results from the exploratory study will be used to determine if the current modeling techniques are adequate to capture the structural response and also aid in the understanding of future test data.

A. Finite Element Model (FEM) of ETU

The FEM was a 39-inch diameter, 45-degree angle sphere cone which consisted of 222,476 elements (primarily solid and shell) with an approximate 0.25 inch element size. A convergence study, focused primarily on local stresses, was performed on the mesh to confirm that the element size was appropriate for the analysis performed. The mesh of the finite element model is shown in Figure 4.

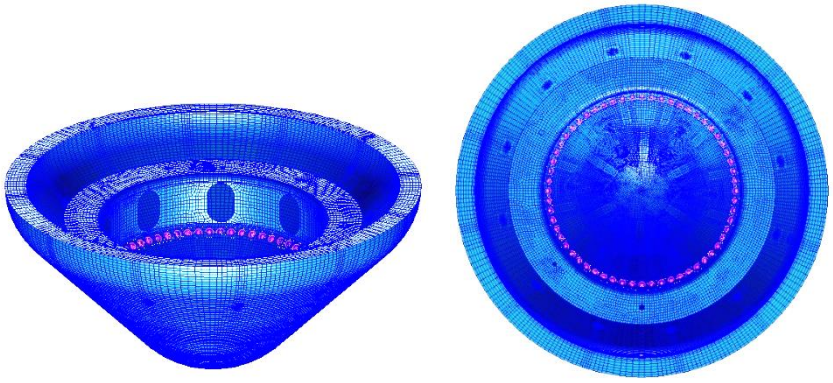

Figure 4. Isometric and interior views of the ETU finite element model mesh.

The HEEET, gap fillers, close-out plugs, and composite carrier structure were modeled with eight-node solid elements and the metallic ring was modeled with shell elements. The HEEET, gap fillers, close-out plugs, and composite carrier structure were modeled as orthotropic materials, and the metallic ring was modeled as isotropic. Previous work has shown that the cold-soak load case is the critical load case for the TTT stresses that cause phenolic microcracking [14]. The differences in material coefficients of thermal expansion (CTE) led to mechanical stress in the ETU when placed under only thermal loading. The large CTE mismatch between the composite carrier structure and metallic ring leads to high TTT stress in the HEEET insulating layer, specifically in the area above the ring attachment. The load case consisted of an initial temperature of 270 °F applied to all nodes. The initial temperature is representative of the adhesive crosslink temperature used in manufacturing and integration of the ETU. A final temperature of -250 °F was applied to all nodes. The final applied temperature was derived as the lowest operational temperature potentially seen during on-orbit transit [14]. The initial and applied nodal temperatures result in a total applied temperature difference of -520 °F. No mechanical loads were applied. Kinematic boundary conditions were applied to eliminate rigid body motion of the model.

The fasteners between the metallic ring and the composite carrier structure were modeled using two-noded CBUSH spring-damper elements [15]. Two different approximations were applied to study the extremes of possible behavior

at the bolted interface. The first approximation was derived using the Huth approximation [16], which is a semi-empirical method used to determine bolted joint stiffness. The second approximation was derived by adjusting the stiffness of the CBUSH elements to match the strain gage results from a thermal cycling test of the composite carrier structure and metallic ring prior to bonding the HEEET material on the outside of the ETU. The Huth approximation resulted in the stiffer of the two joints. The two models will henceforth be referred to as the stiff and soft joint approximations. The effect of these two models on the extent of the phenolic microcracking was analyzed and compared.

B. Analysis Methodology for Iterative Solution of Microcrack Propagation

The macroscopic effect of phenolic microcracking is represented herein as a reduction of stiffness in the material. An iterative linear analysis was performed to predict the extent of the microcracking and the associated load redistribution. First, a linear analysis of the model was performed and any elements in which stress value exceeded a specified microcracking initiation strength in the TTT direction of the insulation layer were identified. An initiation strength of 325 pounds per square inch (psi) was chosen from test data that indicated the stress at which the phenolic microcracking begins [14]. Then, the material properties of these elements were replaced with a reduced stiffness material property. The properties for the reduced stiffness HEEET insulating layer were set by reducing the TTT stiffness modulus to 1000 psi. This reduction is approximately two orders of magnitude. The in-plane and shear material moduli were reduced by the same factor. The intention of the reduction in TTT stiffness was to reduce the stiffness in the TTT direction to a negligible value while avoiding the numerical issues that would result by reducing the stiffnesses to zero. After the properties were replaced, the load case was then re-analyzed with the updated properties. In subsequent iterations, the TTT stress in the intact elements was again compared against an initiation strength, and those that exceeded the initiation strength were assigned reduced properties. In addition, the TTT stress in the elements adjacent to a microcracked element were compared against an assumed propagation strength, which could be lower than the initiation strength. The propagation strength was chosen as an estimate of the stress level at which the phenolic microcracking propagates in intact material that is adjacent to material with microcracks. Two different propagation strengths were studied, one where the propagation strength is equal to the initiation strength, and one where the propagation strength is much lower than the initiation strength. These two strength levels were chosen to provide estimated bounds for the exploratory study because the true propagation strength for the phenolic microcracks was unknown. A propagation strength equal to the initiation strength gathered from test data represented

the upper bound of a propagation strength, and a propagation strength of 50 psi was arbitarily chosen as a minimum bound in the exploratory study. Then, those elements which had exceeded the choosen propagation strength were also assigned reduced properties. The solution process was repeated until the TTT stress in all elements adjacent to other microcracked elements was below the propagation strength. A flow chart of the process is shown below in Figure 5.

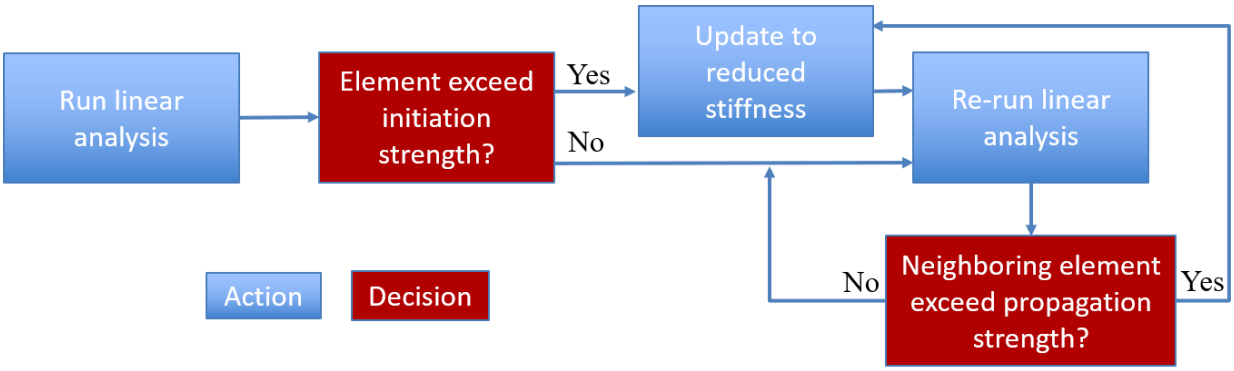

Figure 5 Flow chart depicting the sequence for the iterative linear analysis, actions are labled in blue and decesions are labled in red.

V. Results

The deformation of the ETU under the thermal load case of -520 °F is shown in Figure 6. The critical area for initiation of the phenolic microcracking is in the HEEET insulating layer directly above the attachment point for the metallic ring to the carrier structure. This is caused by the large CTE mismatch between the metallic ring and the composite carrier structure creating relatively large deformation as compared to the rest of the ETU and thus, high TTT stresses in that location. The critical area is circled in red in Figure 6.

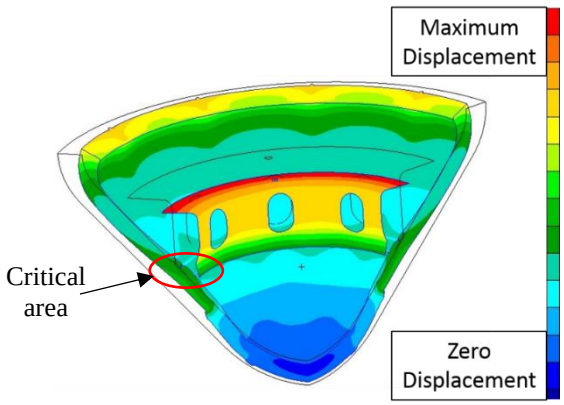

Figure 6. Cutaway view of the ETU deformation (exaggerated) under cold-soak loading. The black outline is the undeformed model and the critical area for initiation of phenolic microcracking in the insulating layer is circled in red.

A. FEM Results

This sub-section will present the results of the linear and iterative linear analyses for four subcases: 1) Stiff joint representation with a 325 psi propagation stress, 2) Stiff joint representation with a 50 psi propagation stress, 3) Soft joint representation with a 325 psi propagation stress, and 4) Soft joint representation with a 50 psi propagation stress. First, the total area of reduced stiffness elements, representing the microcracked phenolic matrix, will be presented along with a comparison of the final TTT stress state in the HEEET insulating layer between the linear and iterative linear analyses.

Case 1: Stiff Joint; 325 psi Propagation Stress

The subcase using the stiff joint representation and 325 psi propagation stress resulted in a small area of reduced stiffness elements centered above the bolted connection on the composite carrier structure. The final reduced stiffness elements are highlighted in Figure 7. The right portion of the figure illustrates the in-plane distribution of the microcracked elements and the cut-away view highlights that the microcracking only propagated through one element through the thickness. The iterative linear solution required twenty-five iterations for the element stiffness reduction to stop propagating.

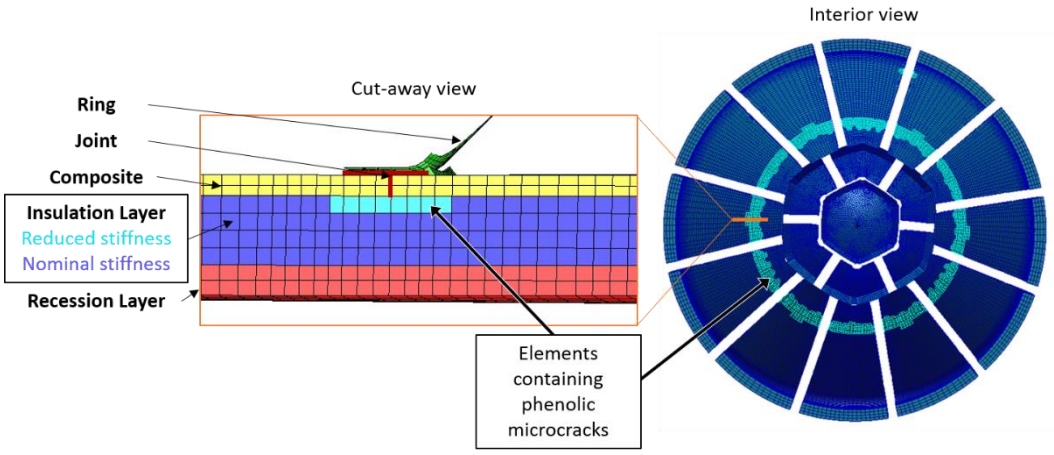

Figure 7. HEEET insulating layer with final reduced stiffness elements highlighted for the stiff joint representation at a 325 psi propagation stress. (Case 1)

The final TTT stress state in the insulation layer for both the linear and iterative linear analyses is shown in Figure 8. The linear analysis was the first analysis of the iterative linear analysis and all the elements in red in the top portion of Figure 8 represent elements that exceeded the initiation strength. The maximum stress near the ring attachment was lower in the iterative linear analysis as compared to the linear analysis that did not take into account phenolic matrix microcracking. The stress levels away from the location that experienced microcracking were unaffected by the microcracking. The ETU did not exceed material allowables in the linear analysis, which assumed pristine material properties and remained below the material allowables throughout the iterative linear analyses. The difference in strains was also compared to determine if there would be a possiblitiy to determine the true behavior of the material from experimental results using strain gages. Due to real-world experimental limitations, only the strains on the recession layer outer mold line and composite carrier structure inner mold line were considered because those were the only viable locations for strain gages to measure the strain. The strains predicted by the linear and the iterative linear analyses at the recession layer outer mold line and the composite carrier structure inner mold line (not shown) are nearly identical. Therefore, strain gage measurements cannot be used at these locations to determine which of the two analyses better represents the experimental results.

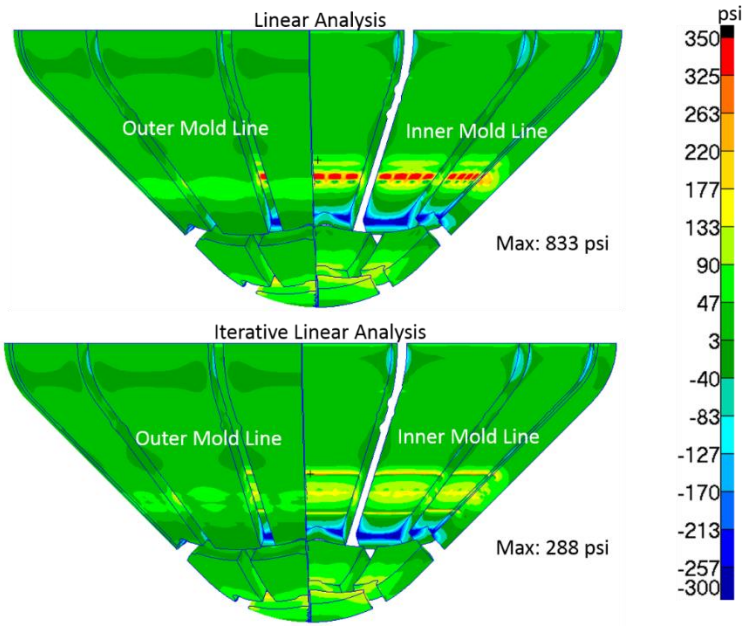

Figure 8. Comparison of TTT stress in the HEEET insulating layer for the stiff joint representation and 325 psi propagating stress. (Case 1)

Case 2: Stiff Joint; 50 psi Propagation Stress

The subcase that assumed the stiff joint representation and 50 psi propagation stress resulted in the entire insulation layer of the outer tile [labeled in Figure 3] becoming reduced stiffness elements. The final reduced stiffness elements are highlighted in Figure 9. The tiles are fully microcracked both in-plane and through the thickness of the tile. After twenty-five iterations of the iterative linear analysis with additional elements continuing to exceed the propagation stress threshold, the entire outer tile was assumed to become completely microcracked and was modeled using the reduced stiffness material property (highlighted below).

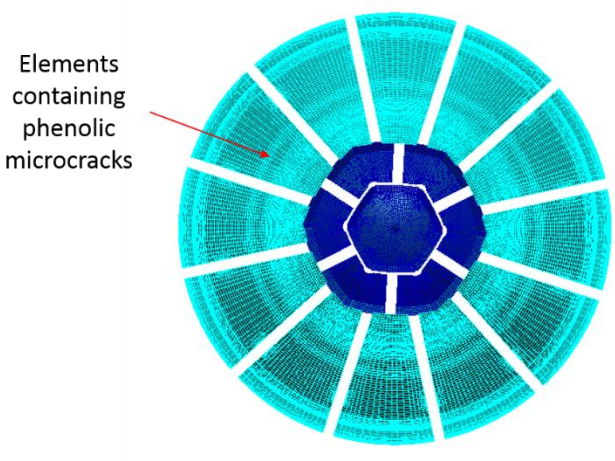

Figure 9. HEEET insulating layer with final reduced stiffness elements highlighted for the stiff joint representation with a 50 psi propagation stress. (Case 2)

The final TTT stress state in the insulation layer for both the linear and iterative linear analyses is shown in Figure 10. The linear analysis was the same as Case 1 (Figure 8) as only the propagation stress was modified and therefore the initial analysis was exactly the same FEM. The maximum stress near the ring attachment was reduced in the iterative linear analysis as compared to the linear analysis with pristine material. However, there were some areas of increased stress in the iterative linear analysis, and there was a difference in the stress contours on the inner tiles, away from the reduced stiffness elements. The differences in stress away from the reduced stiffness elements is in contrast to Case 1, the stiff joint with a 325 psi propagation stress, where there were no differences in the stress away from the microcracked elements as compared to the pristine analysis. Additionally, in Case 2, there were strain differences greater than 50 microstrain at strain gage locations on the outer mold line of the recession layer and inner mold line of the composite carrier. If the entire outer tile experiences phenolic microcracking during testing, the strain gages may be able to measure the strain. The strain gage readings would provide a possible indication that the phenolic microcracks propagated at a lower stress than the 325 psi initiation stress.

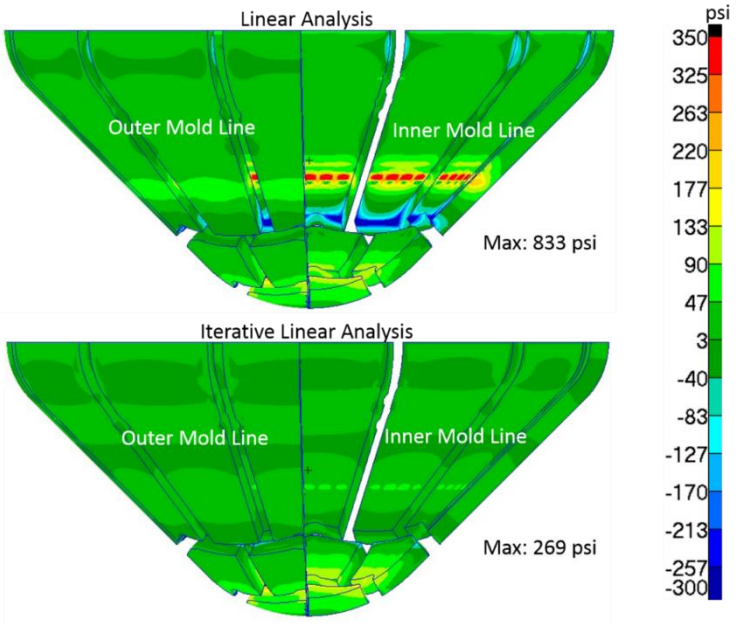

Figure 10. Comparison of TTT stress in the HEEET insulating layer for the stiff joint representation and 50 psi propagating stress. (Case 2)

Case 3: Soft Joint; 325 psi Propagation Stress

The analysis using the soft joint representation and 325 psi propagation stress resulted in a small area of reduced stiffness elements centered on the connection to the bolts, very similar to Case 1. The final reduced stiffness elements for Case 3 are highlighted in Figure 11. The iterative linear solution took seven iterations for the reduced stiffness elements to stop propagating.

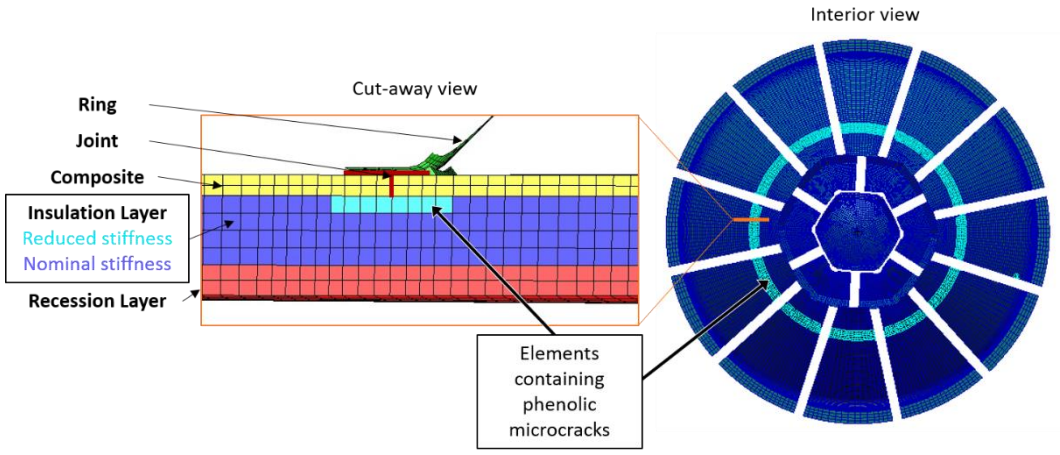

Figure 11. HEEET insulating layer with final reduced stiffness elements highlighted for the soft joint representation with a 325 psi propagation stress. (Case 3)

The final TTT stress state on the inner mold line and outer mold line of the insulation layer for both the linear and iterative linear analyses is shown in Figure 12. As with the stiff joint subcases, the maximum stress was located near the ring attachment and reduced in the iterative linear analysis. The initial linear analysis had lower final stress state than the initial linear analysis of the stiff joint. However, the results from the final iterative linear analysis were similar to the results of the stiff joint with 50 psi propagation stress. The difference in strains on the recession layer outer mold line and composite carrier structure inner mold line were negligible between the linear and iterative linear analysis. Similar to Case 1, the differences in strain were within the accuracy levels of what was able to be measured via strain gages.

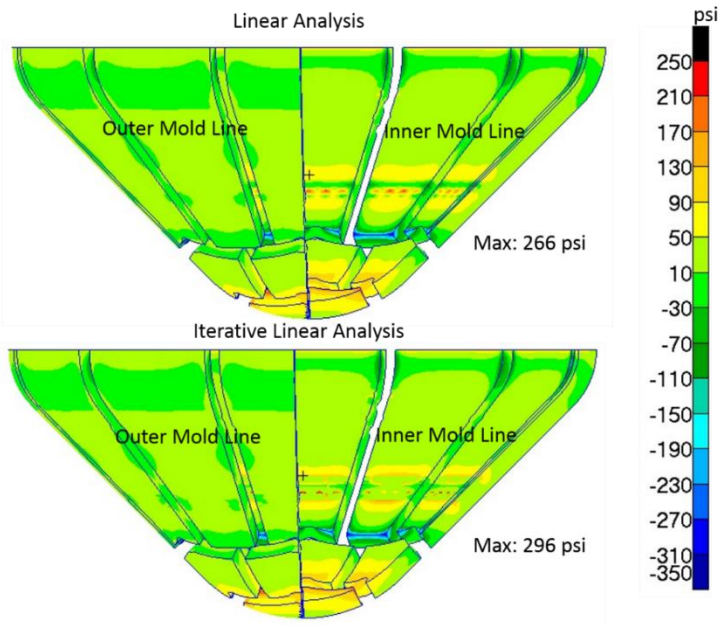

Figure 12. Comparison of TTT stress in the HEEET insulating layer for the soft joint representation and 325 psi propagating stress. (Case 3)

Case 4: Soft Joint; 50 psi Propagation Stress

The subcase using the soft joint representation and 50 psi propagation stress resulted the entire outer tile becoming reduced stiffness elements, the same result as the stiff joint representation and 50 psi propagation stress. The final reduced stiffness elements are highlighted in Figure 13. After twenty iterations of the iterative linear analysis, the entire outer tile was assumed to become reduced stiffness elements.

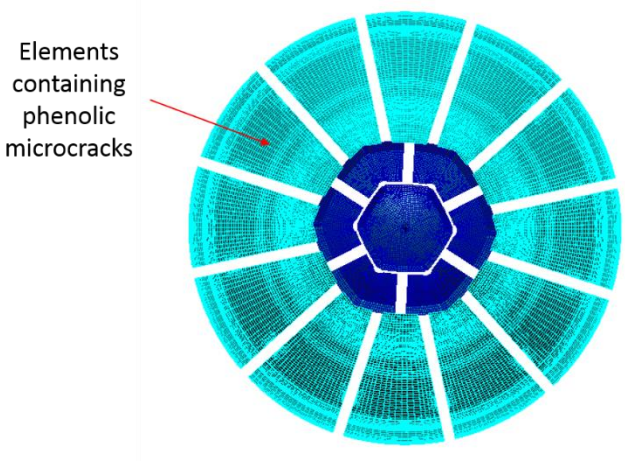

Figure 13. HEEET insulating layer with final reduced stiffness elements highlighted for the soft joint representation with a 50 psi propagation stress. (Case 4)

The final TTT stress state in the insulation layer for both the linear and iterative linear analyses is shown in Figure 14. The maximum stress was increased for the iterative linear analysis, but is reduced at the section near the bolt attachment on the metallic ring. There were also differences in the stress contours on the inner tiles away from the reduced stiffness elements. The strain differences were greater than 50 microstrain at strain gage locations on the outer mold line of the recession layer and inner mold line of the composite carrier. If the entire outer tile experiences phenolic microcracking during the test, the strain gage measurements should give an indication as to which analysis is more accurate.

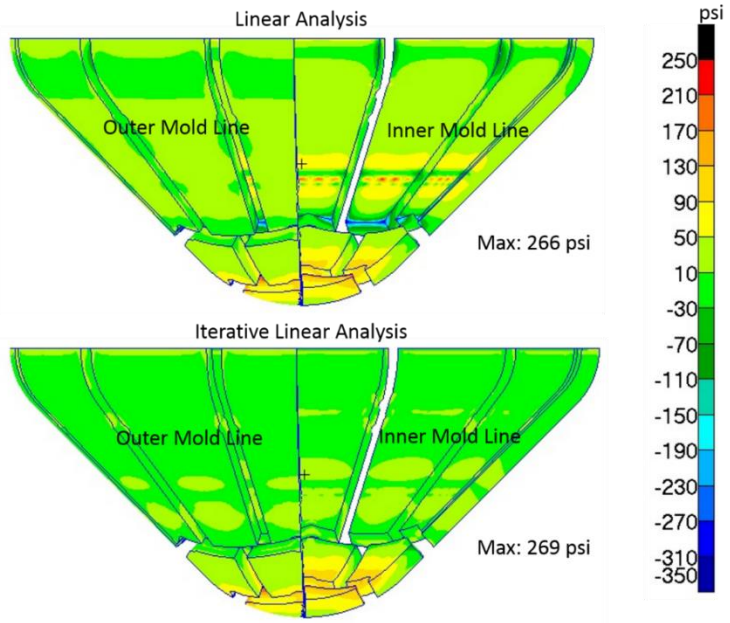

Figure 14. Comparison of TTT stress in the HEEET insulating layer for the soft joint representation and 50 psi propagating stress. (Case 4)

VI.Discussion of Results

The results of the four analysis cases indicate that the predicted final stress state is more dependent on the propagation strength of the microcracking than the joint representation. When the propagation stress was assumed to be equal to the initiation stress (325 psi), the reduction in material stiffness remained localized. When the propagation stress was assumed to be 50 psi, the phenolic microcracking and resulting reduction in material stiffness extended throughout the entire insulation layer of the outer tile. The stiff versus soft joint representations only affected the initial area of elements that exceeded the initiation stress threshold. However, if the joint behaves similarly to the soft joint representation during the test, and the full temperature range of 520°F is not realized, no elements would exceed the 325 psi initiation stress and no phenolic microcracking would occur.

The reduction in material stiffness did not negatively affect any critical material strength allowables as compared to the linear analysis which did not take into account any phenolic microcracking and assumed pristine material properties. An interesting result of the study was that the phenolic microcracking and resulting material stiffness

reduction did not propagate beyond the circumferential HEEET-derived gap fillers. This observation points towards the potential use of the gap filler as a crack arrestor in future designs. Of importance to note, the large TTT stress in the insulating layer above the ring during the cold soak load case was caused only by the CTE mismatch between the materials, which could be eliminated by using a different design, such as a composite ring with a CTE that is more similar to that of the HEEET and composite carrier structure.

The simplified analysis methodology worked well for this exploratory study as a way to investigate the behavior of the microcracked matrix, without having to fully simulate and quantify the microcracks. Future work would include analyzing strain gauge data from the ETU testing to determine if the material behaves in the manner modeled, and which subcase most closely matches the experimental results. There is also a need to better understand and characterize the propagation stress for the phenolic microcracking, as the propagation stress was found to be a critical parameter to determine the extent of the material stiffness reduction. Determination of the propagation stress in the HEEET material could be accomplished with a test similar to a mode I fracture test.

VII. Concluding Remarks

The effect of phenolic microcracking in the HEEET insulating layer and the resulting stress distribution with reduced stiffness elements was studied via a comparison of finite element analysis results based on a linear analysis and an iterative linear analysis. Phenolic microcracking in the insulating layer has been designated as a non-critical failure by the HEEET project, and matrix with microcracks can fully satisfy the thermal requirements. The exploratory study presented confirmed that taking into account the potential load redistribution that results from microcracking does not result in structural failure of the ETU under thermal loading.

Four different subcases were compared: a stiff joint representation with a 325 psi propagation strength, a stiff joint representation with a 50 psi propagation strength, a soft joint representation with a 325 psi propagation strength, and a soft joint representation with a 50 psi propagation strength. The results were primarily dependent on the propagation strength. A propagation strength of 325 psi (which matched the initiation strength) resulted in a localized area of reduced material stiffness centered on the ring attachment. A propagation strength of 50 psi resulted in microcracking around the entire outer tile of the heatshield. The effect of the soft and stiff joint representations was minor, as the joint stiffness affected only the results of the first cycle of the iterative analysis and not the final distribution of microcracking. The simplified analysis methodology used was sufficient for the exploratory study.

A noteworthy outcome of the exploratory study was that the phenolic microcracking never propagated beyond the HEEET-derived gap filler. The lack of microcracking beyond the gap filler points toward a potential to use the gap filler in future designs as a crack arrester. In addition, the TTT stress, which caused the phenolic microcracking in the ETU design, was due to the CTE mismatch between the composite carrier structure and the metallic ring. In future designs, the thermal mismatch could be eliminated by using materials with more similar CTEs.

Acknowledgements

The authors would like to thank and acknowledge the rest of the HEEET team for their work and support of the presented work. The authors would also like to thank the Space Technology Mission Directorates Game Changing Development Program and Science Mission Directorate for their funding of the HEEET project.

References

[1] Blosser, M.L., "Advanced Metallic Thermal Protection Systems for Reusuable Launch Vehicles," Univerisity of Virginia, Charlottesville, VA, 2000.

[2] Strauss, E.L., "Superlight Ablative Systems for Mars Lander Thermal Protection," *Journal of Spacecraft*, Vol. 4, No. 10, 1968, pp. 1304 – 1309. https://doi.org/10.2514/3.29076

[3] Tran, H. K., et. al., "Phenolic Impregnated Carbon Ablators (PICA) as Thermal Protection Systems for Discovery Missions," NASA TM-110440, 1997.

[4] Pavlosky, J.E, and St. Leger, L.G., "Apollo Experience Report – Thermal Protection Subsystem," NASA TN D-7564, NASA Johnson Space Center, Jan 1974.

[5] Wright, M., et. al., "Sizing and Margins Assessment of Mars Science Laboraty Aeroshell Thermal Protection System," *Journal of Spacecraft and Rockets*, Vol. 51, No. 4, July – Aug 2014, pp. 1125-11370. https://doi.org/10.2514/1.A32579

[6] Driver, D.M., et. al., "Arc Jet Testing in a Shear Environment for Mars Science Laboratory Thermal Protection System," 41st AIAA Thermophysics Conference, AIAA Paper 2009-4230, San Antonio, TX, June 2009. https://doi.org/10.2514/6.2009-4230

[7] Bartlett, E.P., Anderson, L.W., and Curry, D.M., "An Evaluation of Ablation Mechanics for the Apollo Heat Shield Material," *Journal of Spacecraft*, Vol. 8, No. 5. , May 1971, pp. 463-469. https://doi.org/10.2514/3.59679

[8] Stewart, M., Koenig, W.J., and Harris, R.F. "Thermal Protection Systems Technology Transfer from Apollo and Space Shuttle to the Orion Program," AIAA SPACE 2018, AIAA Paper 2018-5134, Orlando, FL, Sept. 2018. https://doi.org/10.2514/6.2018-5134

[9] Rose, C.A., Davilia, C.G., and Leone, F.A., "Analysis Methods for Progressive Damage of Composite Structures," NASA-TM-2013-218024, July 2013.

[10] Kilic, H., and Haj-Ali, R., "Progressive Damange and Nonlinear Analysis of Pultruded Composite Structures," *Composites Part B: Engineering*, Vol. 34, No. 3, April 2003, pp. 235-250. https://doi.org/10.1016/S1359-8368(02)00103-8

[11] Hult, J., "Introduction and General Overview," *Continuum Damange Mechanics Theory and Application*, Springer-Verlag Wein, 1987, pp. 1-35. https://doi.org/10.1007/978-3-7091-2806-0_1

[12] Maimi, P, Camanho, P.P., Mayugo, J. A., and Davilia, C.G., "A Continuum Damage Model for Composite Laminates: Part I – Constitutive Model," *Mechanics of Materials*, 2007, pp. 897-908. https://doi.org/10.1016/j.mechmat.2007.03.005

[13] Hyder, I, et. al., "Implementation of a Matrix Crack Spacing Parameter in a Continuum Damage Mechanics Finite Element Model," 33rd American Society for Composites, Seattle, WA, Sept. 2018. https://doi.org/10.12783/asc33/26052

[14] "HEEET Final Report: Design Data Book Executive Summary," HEEET-1004, NASA Ames Research Center, Code TS Entry Systems, May, 2019.

[15] Anon, MSC Nastran 2012.2 Quick Reference Guide, Santa Ana, CA: MSC Software Corporation, 2012.

[16] Huth, H., "Influence of Fastener Flexibility on the Prediction of Load Transfer and Fatigue Life for Multiple-Row Joints," *Fatigue in Mechanically Fastened Composite and Metallic Joints*, West Conshohocken, PA, ASTM International, 1986, pp. 221-230. https://doi.org/10.1520/STP29062S